Time-Scaling Modeling and Control of Robotic Sewing System

Kai Tang, *Student Member, IEEE*, Fuyuki Tokuda, *Member, IEEE*, Akira Seino, *Member, IEEE*, Akinari Kobayashi, *Member, IEEE*, Norman C. Tien, and Kazuhiro Kosuge, *Life Fellow, IEEE*

***Abstract*—Automating the sewing process presents significant challenges due to the inherent softness of fabrics and the limited control capabilities of sewing systems. To realize sewing automation, we propose a time-scaling modeling and control architecture of the robotic sewing system. By using the time-scaling modeling, the nonholonomic kinematics of the sewing process of the industrial sewing machine is linearized precisely. Based on this model, a two-layer real-time control architecture is proposed. The upper layer controls the sewn seam line trajectory using the model-based feedback control implemented in the time-scaling domain, while the lower layer controls the manipulator and the sewing machine using geometric-based trajectory generation and coordinated motion control of the robot and the sewing system in the time domain. The experimental results demonstrate that the sewing trajectories exponentially converge to the desired trajectories without overshooting under different initial conditions and sewing speeds. Besides, the same sewing trajectories under different sewing speeds are obtained for a given stitch size. The sewing results show the good performance and application potential of the proposed robotic sewing system.**

***Index Terms*—Feedback control, force control, linearization, manipulator, sewing automation, time-scaling modeling.**

Manuscript received 19 January 2024; revised 26 March 2024; accepted 3 May 2024. Date of publication 21 May 2024; date of current version 16 August 2024. Recommended by Technical Editor J. She and Senior Editor Q. Zou. This work was supported in part by the JC STEM Lab of Robotics for Soft Materials funded by The Hong Kong Jockey Club Charities Trust and in part by the Innovation and Technology Commission of the HKSAR Government under the InnoHK initiative. *(Corresponding author: Kai Tang.)*

Kai Tang, Fuyuki Tokuda, Akira Seino, Akinari Kobayashi, and Norman C. Tien are with the Department of Electrical and Electronic Engineering, Faculty of Engineering, The University of Hong Kong, Hong Kong SAR, China, and also with the Centre for Transformative Garment Production, Hong Kong SAR, China (e-mail: tangkai@eee.hku.hk; fuyuki.tokuda@transgp.hk; akira.seino@transgp.hk; akinari.kobayashi@transgp.hk; nctien@transgp.hk).

Kazuhiro Kosuge is with the Department of Electrical and Electronic Engineering, Faculty of Engineering, The University of Hong Kong, Hong Kong SAR, China, and with the Centre for Transformative Garment Production, Hong Kong SAR, China, and also with the JC STEM Lab of Robotics for Soft Materials, Department of Electrical and Electronic Engineering, Faculty of Engineering, The University of Hong Kong, Hong Kong SAR, China (e-mail: kosuge@hku.hk).

This article has supplementary material provided by the authors and color versions of one or more figures available at https://doi.org/10.1109/TMECH.2024.3398713.

Digital Object Identifier 10.1109/TMECH.2024.3398713

I. Introduction

As a vital procedural component in garment production, sewing accounts for approximately 80% of the fabric linkages and about 40% of the total production cost [1]. The quality of sewn articles is closely related to the proficiency of sewing operators in manipulating the fabric parts during sewing. High-level skills are required to ensure sewing at desired locations and prevent undesirable wrinkles or seam puckering, both of which could lead to defective products.

Among various automation technologies, the use of robots offers immense potential to substitute manual sewing operations. Several robotic sewing companies, such as Softwear, PFAFF Industrial, and Sewbo, have incorporated different robots in their automated sewing systems to tackle the fabrication of different types of garment or upholstery articles. However, sewing automation is still a challenging problem due to the following two main issues [2], [3].

1) Fabric, as a soft material, has a highly nonlinear morphology whose state completely depends on the environment and the history of the manipulation. This property makes the modeling difficult for real-time task requirements.
2) The fabric has infinite states, while the number of sensors and actuators of an automation system is limited, which makes the sewing task a partially observable and underactuated control problem.

Several research studies have been conducted on the automatic sewing process. Gershon et al. [4] decomposed the sewing task into four concurrent processes including the sewing process, feeding process, tension process, and contour process. Although each subtask is modeled by a simple linearized model, relatively robust results were obtained. Koustoumpardis et al. [5] focused on the fabric tension control of the sewing task by designing a hierarchical control strategy based on a fuzzy control scheme. Winck et al. [6] proposed an automated sewing cell that has a newly designed fabric feeding machine. Based on the experimental results, the necessity of the feedback control scheme is discussed in their literature. Schrimpf et al. [7], [8] presented a robotics sewing platform for a leather edge sewing task. The edge sensor can detect the positions of the upper and lower leather, which are the feedback of the sewing direction control. Recently, Tokuda et al. [9] realized automated sewing by synchronizing the needle sewing speed and fabric motion using the dual manipulator system, which highlights the importance of synchronization between manipulators and sewing machine.

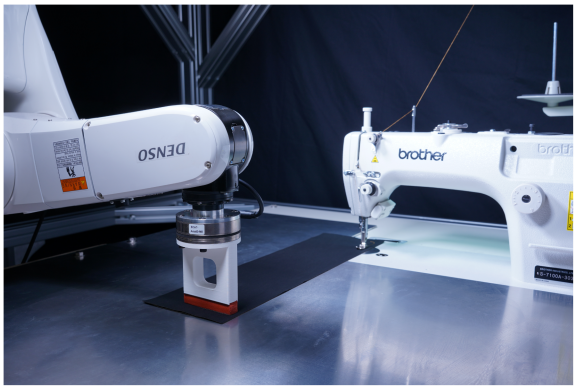

Fig. 1. Proposed robotic sewing system, including a manipulator and an industrial sewing machine, enables the sewing along the desired seam line of the two layers of aligned woven fabrics.

More research in [10], [11], [12], and [13] provides valuable references for sewing automation and shows the importance of the combination of feedback and force control for underactuated sewing tasks.

However, to the best of authors' knowledge, no existing research considers the kinematics of the sewing process precisely. In addition, existing automated sewing controllers do not consider the ease of use and robustness under different initial conditions and sewing speeds. This article proposes the kinematics modeling of the sewing process, which simplifies the controller design while maintaining high accuracy. Based on the proposed model, a general and easily deployable control architecture is proposed. Several experiments are conducted to demonstrate the performance of the proposed control scheme. The contribution of this article can be summarized as follows.

1) The kinematics of the sewing process are modeled as a nonholonomic process and linearized precisely by the time-scaling technique.
2) An experimental platform and a real-time control architecture are proposed based on the time-scaling modeling of the sewing process kinematics.
3) Experimental results show the high performance and application potential of the proposed robotic sewing system.

The rest of this article is organized as follows. Section II presents the experimental platform, including hardware and coordinate frames used for the modeling and control of the robotic sewing system. The modeling of the sewing process kinematics is illustrated in Section III, and the control architecture is proposed in Section IV. Experimental results are shown in Section V. Finally, Section VI concludes this article.

II. Experimental Robotic Sewing Platform

This section provides an overview of the experimental robotic sewing platform shown in Fig. 1 and the coordinate frames used for the modeling and control of the robotic sewing platform.

A. Hardware

The robotic sewing platform consists of an industrial sewing machine, a 6-DoF manipulator, a force and torque sensor (F/T sensor), a vision sensor, and a controller PC.

1) Industrial Sewing Machine: The industrial sewing machine (Brother Industries S7100-A) is mounted to an aluminum frame via the sewing machine level table. Note that the manipulator and the high-speed vision system are also attached to this aluminum frame to fix their geometric relations. To control the sewing machine by the controller PC easily, the motor of the sewing system was replaced by an AC servo motor (Yaskawa Electric SGM7A), which is controlled by a servo controller (Yaskawa Electric SGD7S) connected to the controller PC via EtherCAT.

During the sewing process, the sewing machine engages and feeds the fabrics through a presser foot and a feed dog. The presser foot is adjusted to ensure the flatness of the fabric around the sewing needle. Due to the circular motion of the feed dog, the fabric is fed forward a predefined distance in each cycle. The fed forward direction is defined as the sewing direction, while the predefined distance is referred to as the stitch size, $\bar{s} \in \mathbb{R}_+$, which can be adjusted before the sewing task using the function of the sewing machine.

2) Manipulator: A 6-DoF manipulator (Denso VS-068) is suspended from the aluminum frame. Meanwhile, the wrist F/T sensor and end-effector are attached to the manipulator to press down the fabric on the table to create line and plane contact, which helps maintain the shape of the material during the sewing process [14]. The manipulator is connected to the controller PC via EtherCAT.

3) F/T Sensor: The wrist F/T sensor (ATI Axia80-M8) is attached to the manipulator and utilized in this platform to estimate the internal force of the fabric and the external force applied to the end-effector during the sewing process. The F/T sensor is connected to the EtherCAT through the manipulator controller in a series way.

4) Vision Sensor: A high-speed camera (Photron INFINICAM UC-1) is mounted on the frame and streams at a resolution of 624×1246 pixels via USB to the Windows OS of the controller PC. This sensor is applied to estimate the distance from the needle insertion point to the closest point on the desired seam line.

5) Controller PC: The controller PC is configured with a 64 GB RAM, an NVIDIA GeForce RTX 3090 GPU, and the Intel(R) Xeon(R) W-2255 CPU. Four cores and six cores of the CPU are assigned for Windows OS and INtime OS, respectively. These operation systems are communicated through an allocated shared memory.

B. Coordinate Frames

The coordinate configuration of this system is shown in Fig. 2. We define the world coordinate frame $o_w - x_w y_w z_w$ denoted as Σ_w, which is fixed to the environment. The direction of y_w and z_w toward that of the sewing direction and the upward normal of the sewing table, respectively. In addition, we define the base coordinate frame $o_b - x_b y_b z_b$ denoted as Σ_b attached to the base joint of the manipulator. We define the camera coordinate frame $o_c - x_c y_c z_c$ denoted as Σ_c, which is attached to the vision sensor. Note that all coordinate frames are defined with reference to Σ_w.

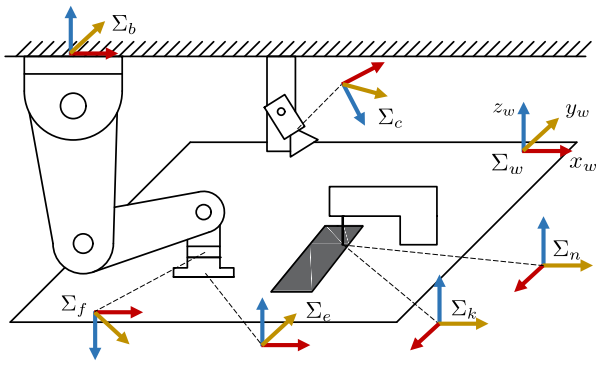

Fig. 2. Robotic sewing platform and its coordinate frames. The red, yellow, and blue axes in the figure correspond to the x, y, and z axes of their respective coordinate frames.

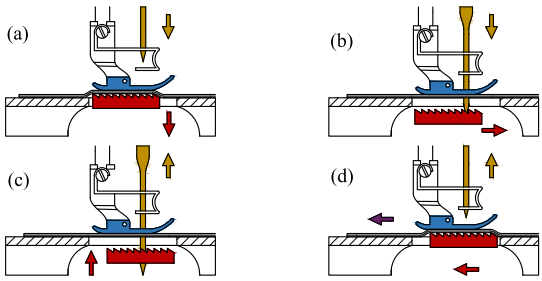

Fig. 3. Sewing process of an industrial sewing machine. The red, yellow, and blue segments correspond to the feed dog, sewing needle, and presser foot, respectively, with their corresponding movement directions in each state. In addition, the purple arrow denotes the fabric's movement direction in state (d), which is defined as the sewing direction.

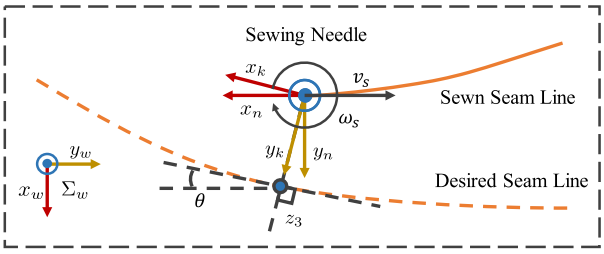

Fig. 4. Definition of Σ_n, Σ_k, and θ for a given sewing needle point and desired seam line. x_n toward the opposite sewing direction and x_k toward the tangent of the desired seam line at the closest point to the needle. v_s and ω_s are defined as the sewing speed in y_w and rotation speed around z_n.

Concerned with the sewing process, we define the needle coordinate frame $o_n - x_n y_n z_n$ denoted as Σ_n attached to the needle insertion point. The direction of x_n is defined as the opposite direction of the sewing direction. The direction of z_n is the same as that of the upward normal of the sewing table.

Another coordinate frame $o_k - x_k y_k z_k$ denoted as Σ_k is defined for the time-scaling modeling. Σ_k is located at the same location of Σ_n while rotated about z_n by an angle of θ. This angle is defined as the angle between the sewing direction and the tangent line to the desired seam line at the point closest to the needle. The definition of Σ_n and Σ_k is shown in Fig. 4.

Furthermore, we define the force sensor coordinate frame $o_f - x_f y_f z_f$, denoted as Σ_f, which is attached to the endpoint of the force sensor. We define the end-effector coordinate frame $o_e - x_e y_e z_e$, denoted as Σ_e, which is attached to the endpoint of the end-effector.

III. Time-Scaling Modeling of Sewing Kinematics

In this article, the sewing process of the industrial sewing machine is emphasized as the motion of the fabric under the combined action of the feed dog, presser foot, and needle rather than the process of stitch formation by the thread during sewing. This process is illustrated in Fig. 3 and is analyzed and modeled in this section.

The sewing cycle to produce a single stitch can be separated by four distinct states defined by the positions of the feed dog and the needle shown in Fig. 3. State (a) is the beginning of each cycle, in which the positions of the feed dog and the needle are the highest. The simultaneous descending of the feed dog and needle follows state (a), and the needle is inserted into the fabric until it reaches state (b), where the feed dog is in its lowest position. The feed dog then starts a reverse movement in the opposite sewing direction while the needle continues its descent to the lowest point, completing the insertion at state (c). Then, both the feed dog and sewing needle ascend to reach state (d), in which the feed dog starts to engage the fabric. Then, a small section of fabric between the feed dog and the presser foot is moved forward in the sewing direction until the system returns to the state (a). By reinserting the needle, a stitch of a predetermined size is formed.

In a sewing cycle, the sewing angle θ defined in Section II-B can only be altered between states (b) and (c) when the feed dog and presser foot are separated, allowing for rotation within a limited range of the fabric around the needle because of mechanical constraints. One cycle of state transition forms one stitch, and the repetitive iteration of state transitions produces a continuous seam line. Fig. 4 shows the definition of sewing direction and θ. Considering the general sewing task, when the length of each stitch is much smaller than the whole sewing length, the kinematics of the sewing process are modeled as a continuous nonholonomic process shown as follows:

$$\frac{d}{dt}\begin{bmatrix} x \\ y \\ \theta \end{bmatrix} = \begin{bmatrix} -\cos\theta \\ -\sin\theta \\ 0 \end{bmatrix} v_s + \begin{bmatrix} 0 \\ 0 \\ 1 \end{bmatrix} \omega_s \tag{1a}$$

$$\text{s.t.: } \dot{x}\sin\theta - \dot{y}\cos\theta = 0 \tag{1b}$$

where x is the current needle position in x_k, y is the distance from the current needle position to the desired seam line in y_k, v_s is the sewing speed in the sewing direction, and ω_s is the rotation speed of the fabric around the needle, z_n.

Note that the proposed model represented by (1) describes the motion of the needle insertion points on the fabric under the following assumptions.

1) The stitch size is predefined and constant during the entire sewing process.
2) There is no translational motion perpendicular to the sewing direction during the sewing process.

Subsequently, the time-scaling approach [15], [16] is introduced to (1) to have a precise and linearized representation of the sewing process and to facilitate the design of the controller. Let us consider a nonlinear system with the state transition $f(t, \boldsymbol{\xi}(t), \boldsymbol{u}(t))$, then, the time-scaling model is defined as

$$\frac{d\boldsymbol{\xi}}{d\tau} = f(\tau, \boldsymbol{\xi}(\tau), \boldsymbol{u}(\tau))\eta(\boldsymbol{\xi})^{-1} \tag{2a}$$

$$\frac{dt}{d\tau} = \frac{1}{\eta(\boldsymbol{\xi})} \tag{2b}$$

where $\boldsymbol{\xi} \in \mathbb{R}^n$ and $\boldsymbol{u} \in \mathbb{R}^m$ are state and input vectors of the system, respectively, the variable $\tau \in \mathbb{R}$ is defined as the time scale variable, and the function $\eta(\boldsymbol{\xi})$ is defined as the continuous time-scaling function. (2) are satisfied if τ is monotonically increasing (or decreasing) and $0 < \eta(\boldsymbol{\xi}) < \infty$ (or $-\infty < \eta(\boldsymbol{\xi}) < 0$).

To derive the time-scaling modeling for (1), a coordinate transformation, $z_1 = x$, $z_2 = \tan\theta$, $z_3 = y$, is applied to (1). Then, we have the following chained form which enables exact linearization of the state transformation after time-scaling [17]. The corresponding transformed inputs are shown as follows: $v_1 = -v_s \cos\theta$ and $v_2 = \omega_s / \cos^2\theta$. Thus, the chained form representation of the sewing process kinematics is given by

$$\dot{z_1} = v_1 \tag{3a}$$

$$\dot{z_2} = v_2 \tag{3b}$$

$$\dot{z_3} = z_2 v_1. \tag{3c}$$

Then, the time-scaling kinematics can be obtained by introducing the time scale variable $\tau = z_1$ and the time-scaling function $\eta(\boldsymbol{\xi}) = v_1(z_1)$, satisfying the relation

$$\frac{dt}{dz_1} = \frac{1}{v_1} \tag{4}$$

subject to the constraint $0 < v_1(z_1) < \infty$. Note that z_1 is the distance traveled by the needle along the desired seam line. By multiplying both sides of the chained form (3) by (4), the kinematics model is transferred from the time domain to z_1 domain, and the linear state-space model of sewing process kinematics is presented as follows:

$$\frac{d}{dz_1}\begin{bmatrix} z_3 \\ z_2 \end{bmatrix} = \begin{bmatrix} 0 & 1 \\ 0 & 0 \end{bmatrix}\begin{bmatrix} z_3 \\ z_2 \end{bmatrix} + \begin{bmatrix} 0 \\ 1 \end{bmatrix}\mu_2 \tag{5a}$$

$$\frac{dz_1}{dt} = \mu_1 \tag{5b}$$

where $\mu_1 = v_1$ and $\mu_2 = v_2/v_1$ are defined as new inputs of the time-scaling model for linearization purposes. Note that z_1 defined as a new time scale variable is valid only if $\mu_1 > 0$, and the coordinate transformation is valid only if $-\pi/2 < \theta < \pi/2$, which makes z_1 monotonically increase as time t increase.

By the time-scaling, the nonholonomic process is exactly linearized in the z_1 domain which facilitates the design of the control input μ_2 to stabilize the system. In this article, we use state feedback to stabilize the system as shown later. Other control strategies can be used to stabilize the system in the z_1 domain.

IV. Real-Time Sewing Control Architecture

Inspired by the manual operation of skilled sewers during the sewing process, we utilize the full functionality of the sewing machine and propose the following control scheme of the robotic sewing platform to emulate the human operation. The human operation involves tracking the feeding motion of the fabrics generated by the sewing machine, rotating fabrics around the needle to control the sewing direction, and controlling the force applied to the fabrics to remove wrinkles.

In the proposed robotic sewing platform, the sewing is carried out by controlling the sewing direction, while the stitch size is predefined and constant during the entire sewing process. During the sewing process, one side of the aligned fabrics is engaged between the presser foot and the feed dog. The sewing machine sews the aligned fabrics with a given sewing speed. At the same time, the manipulator presses the other side of the fabrics on the sewing table to create static friction between the end-effector and the upper fabric, and the upper fabric and the lower fabric.

During the sewing process, the end-effector follows the feeding motion of the aligned fabrics to maintain the relative velocity between the end-effector and the aligned fabrics zero and control the fabrics' internal force to prevent wrinkles, bunching, and puckering. The feeding direction of the aligned fabrics is controlled by the end-effector's rotational motion.

To implement the described sewing process, a real-time control architecture shown in Fig. 5 is proposed with two control layers, the upper layer, and the lower layer. The upper layer operated under the Windows OS controls the sewn seam line trajectory in the z_1 domain by applying model-based feedback control to the proposed time-scaling model (5). The lower control layer operated under the INtime OS in the time domain is implemented for the following two primary objectives.

1) To control the feeding direction of the fabrics and synchronize the end-effector's motion with the sewing velocity using geometric-based trajectory generation.
2) To dynamically control the internal force of the fabric and the external force applied to the end-effector by using the coordinated motion control of the robot and the industrial sewing machine.

A. Model-Based Feedback Control

The model-based feedback control is designed to stabilize the time-scaling modeling of the sewing process kinematics, to obtain the rotation speed ω_s of the fabric around the sewing needle, for a given sewing speed v_s, and a given stitch size $\bar{s}$. The relation between v_s and $\bar{s}$ is expressed as follows:

$$v_s = \bar{s}\Lambda \tag{6}$$

where $\Lambda \in \mathbb{R}_+$ is the number of stitches per second, which is adjusted based on a trapezoid profile with short warm-up and cold-down sections and a given constant sewing speed $\bar{n}_s$.

The rotation speed ω_s is calculated based on the model-based feedback control in the z_1 domain. We assume that $z_2(z_1)$ and $z_3(z_1)$ are estimated by the vision sensor. Then, based on the proposed sewing process kinematics (5), a feedback controller

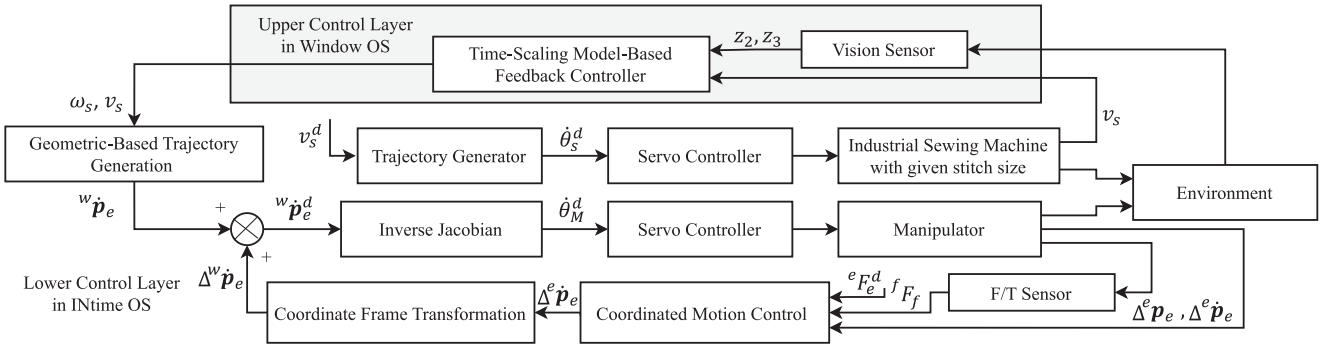

Fig. 5. Block diagram of the real-time control architecture, with the grey square being the upper layer controlled in the time-scaling domain, while the lower layer controlled in the time domain. Velocity control mode is employed for the servo controllers of both the industrial sewing machine and manipulator. The desired sewing speed is denoted by v_s^d, while ${}^w\dot{\boldsymbol{p}}_e^d$ represents the desired twists of the end-effector in Σ_w. The desired joint velocities of the industrial sewing machine and the manipulator are given by $\dot{\theta}_s^d$ and $\dot{\theta}_M^d$, respectively.

to stabilize the system in the z_1 domain is designed as follows:

$$\mu_2(z_1) = -K[z_3(z_1),\, z_2(z_1)]^\top \tag{7}$$

where $K = [k_3,\, k_2] \in \mathbb{R}_+^2$ is defined as the state feedback gain. The system is controllable, and the state feedback gain to stabilize the system can always be obtained using the pole assignment technique, etc. Therefore, using the relation $\mu_2 = v_2/v_1$, v_2 is calculated as follows:

$$v_2 = -k_2 z_2 v_1 - k_3 z_3 v_1. \tag{8}$$

Finally, the rotation speed, $\omega_s = v_2 \cos^2\theta$, is calculated for rotational motion control in the lower control layer.

B. Geometric-Based Trajectory Generation

The geometric-based trajectory generation calculates the end-effector's motion so that the rotational motion of the fabrics around the sewing needle, and the feeding motion synchronization of the end-effector with the fabrics feeding motion of the sewing machine are assured. Note that the geometric-based trajectory generation is calculated in the world coordinate frame Σ_w.

Let us define ${}^w\boldsymbol{x}_e = [{}^w x_e, {}^w y_e, {}^w z_e]^\top \in \mathbb{R}^3$ and ${}^w\boldsymbol{x}_n = [{}^w x_n, {}^w y_n, {}^w z_n]^\top \in \mathbb{R}^3$ as the position of the origin of the coordinate frame Σ_e and Σ_n with reference to Σ_w. Let us define ${}^w\dot{\boldsymbol{p}}_e = [{}^w\boldsymbol{\omega}_e^\top, {}^w\boldsymbol{v}_e^\top]^\top \in \mathbb{R}^6$ be the end-effector twist, which consists of angular velocity ${}^w\boldsymbol{\omega}_e^\top \in \mathbb{R}^3$ and velocity ${}^w\boldsymbol{v}_e^\top \in \mathbb{R}^3$ with reference to Σ_w. The angular velocity of the end-effector around the sewing needle ${}^w\boldsymbol{\omega}_e^\top = [0, 0, \omega_s]$ is given from the upper layer. Then, the velocity of the end-effector with reference to Σ_w can be calculated as follows:

$${}^w\boldsymbol{v}_e = ({}^w\boldsymbol{x}_e - {}^w\boldsymbol{x}_n) \times {}^w\boldsymbol{\omega}_e. \tag{9}$$

The feeding motion synchronization of the end-effector is applied along the y_w axis of the world coordinate frame Σ_w to provide a desired velocity of the end-effector. The synchronized feeding motion is calculated as follows:

$${}^w\dot{y}_e = \gamma\, v_s \tag{10}$$

where $\gamma \in (0, 1]$ is defined as the scaling factor to synchronize the velocity of the end-effector to the actual sewing velocity of the industrial sewing machine.

C. Coordinated Motion Control

A force control scheme is designed based on the concept of the virtual mechanism [18], to control the internal force of the fabric and the external force applied to the end-effector [19]. Let us define ${}^f\boldsymbol{F}_f = [{}^f\boldsymbol{\tau}_f^\top, {}^f\boldsymbol{f}_f^\top]^\top \in \mathbb{R}^6$ as the body wrench which consists of torque ${}^f\boldsymbol{\tau}_f \in \mathbb{R}^3$, and force ${}^f\boldsymbol{f}_f \in \mathbb{R}^3$, detected by the F/T sensor with reference to the force sensor coordinate frame Σ_f. Then, the body wrench applied to the end-effector with reference to the end-effector coordinate frame Σ_e can be calculated as follows:

$${}^e\boldsymbol{F}_e = \left[Ad_{fT_e}\right]^\top {}^f\boldsymbol{F}_f \tag{11}$$

where $\left[Ad_{fT_e}\right]^\top \in \mathbb{R}^{6\times 6}$ as the adjoint representation of the force transformation from Σ_f to Σ_e is calculated as follows:

$$\left[Ad_{fT_e}\right]^\top = \begin{bmatrix} {}^e\boldsymbol{R}_f & -{}^e\boldsymbol{R}_f \left[{}^f\boldsymbol{x}_e\times\right] \\ 0 & {}^e\boldsymbol{R}_f \end{bmatrix} \tag{12}$$

where ${}^e\boldsymbol{R}_f \in \mathbb{R}^{3\times 3}$ is the rotation matrix and $\left[{}^f\boldsymbol{x}_e\times\right]$ is the skew-symmetric matrix representation of the position of Σ_e with reference to Σ_f shown as follows:

$$\left[{}^f\boldsymbol{x}_e\times\right] = \begin{bmatrix} 0 & -{}^f z_e & {}^f y_e \\ {}^f z_e & 0 & -{}^f x_e \\ -{}^f y_e & {}^f x_e & 0 \end{bmatrix}. \tag{13}$$

The internal force of the fabric and the external force of the end-effector are controlled based on the impedance control laws for the dynamics of the virtual mechanism such that

$$\boldsymbol{M}\Delta^e\ddot{\boldsymbol{p}}_e + \boldsymbol{D}\Delta^e\dot{\boldsymbol{p}}_e + \boldsymbol{K}\Delta^e\boldsymbol{p}_e = \boldsymbol{S}\left({}^e\boldsymbol{F}_e - {}^e\boldsymbol{F}_e^d\right). \tag{14}$$

where $\boldsymbol{M} \in \mathbb{R}^{6\times 6}$, $\boldsymbol{D} \in \mathbb{R}^{6\times 6}$, and $\boldsymbol{K} \in \mathbb{R}^{6\times 6}$ are apparent inertia, damping, and stiffness matrices, respectively. Note that the impedance control law in the sewing direction can be designed to ensure that the tension of the fabric is less than the maximum value $\mathcal{T}_{\max}$, which prevents unacceptable stretching deformation during the entire sewing process. $\Delta^e\boldsymbol{p}_e \in \mathbb{R}^6$ is

TABLE I
PARAMETERS OF COORDINATED MOTION CONTROL

Parameters	Value
${}^e\boldsymbol{F}_e^d$	$[0, 0, 0, 0, 0, 5]^\top$
$\boldsymbol{S}$	$\mathbf{diag}(1, 1, 1, 0, 1, 1)$
$\boldsymbol{M}$	$\mathbf{diag}(2.5, 5.0, 5.0, 0, 0.0001, 0.1)$
$\boldsymbol{K}$	$\mathbf{diag}(5000, 5000, 5000, 0, 0, 0)$
$\boldsymbol{D}$	$\mathbf{diag}(10000, 30000, 30000, 0, 220, 1000)$

the displacement of the end-effector from the nominal pose regarding Σ_e, and the nominal pose is calculated based on the geometric-based trajectory generation scheme proposed in the previous section, ${}^e\boldsymbol{F}_e^d \in \mathbb{R}^6$ is the desired external force of the end-effector with reference to the end-effector coordinate Σ_e, and $\boldsymbol{S} = \mathbf{diag}(\lambda_1, \lambda_2, \ldots, \lambda_6) \in \mathbb{R}^{6\times 6}$ is defined as a selection matrix with each element defined as follows:

$$\lambda_i = \begin{cases} 1, & \text{if the } i\text{th coordinate in impedance mode} \\ 0, & \text{if the } i\text{th coordinate in position mode.} \end{cases} \tag{15}$$

Then, $\Delta^e\dot{\boldsymbol{p}}_e$ can be transformed to the world coordinate frame Σ_w calculated by the relation: $\Delta^w\dot{\boldsymbol{p}}_e = [Ad_{wT_e}]\Delta^e\dot{\boldsymbol{p}}_e$, where $[Ad_{wT_e}]$ is the adjoint representation defined with the same form as (12). Then, the transformed displacement is combined with the trajectory generated in Section IV-B for manipulator real-time control.

V. EXPERIMENTAL RESULTS

This section provides experimental results to demonstrate the validity of the proposed time-scaling modeling of the sewing process and to show the performance of the proposed robotic sewing system with the real-time control architecture.

In the experiments, the desired seam line is defined with a 20 mm margin size from the fabric's edge. Two pieces of square woven fabrics, with the size of 140 × 500 mm in solid black color, are selected for a linear desired seam line, while two pieces of woven fabrics with an s-shape edge of 420 mm radius are selected for a curved desired seam line. The procedure of an experiment is shown as follows.

1) One side of the two aligned fabrics is placed between the presser foot and feed dog for a given initial state.
2) The end-effector presses down at the end of the aligned fabrics on the table by external force control.
3) The system sews the fabrics by tracking the desired seam line based on the proposed control architecture.
4) The sewing process ends after sewing a predefined distance along the desired seam line.

The stitch size $\bar{s}$ is set to 2.4 mm. The scaling factor is set to $\gamma = 0.9$ based on preliminary experiments. The upper and lower threads are selected with a diameter of about 0.3 mm. k_3 and k_2 are selected equal to 0.0029 and 0.1085 by pole placement based on the maximum rotation speed of the sewing process, ensuring the desired trajectory's convergence without overshoot. The maximum tension of the fabric $\mathcal{T}_{\max} = 3$ N. The parameters of coordinated motion control shown in Table I are experimentally selected and kept constant to ensure wrinkle-free fabric and stable interaction between the end-effector and environment in different sewing tasks.

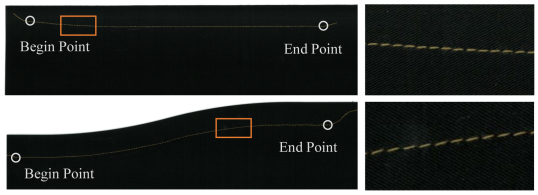

Fig. 6. Scan photos of the sewing result of Sc1 (up) and Sc8 (low) and their corresponding enlarged results.

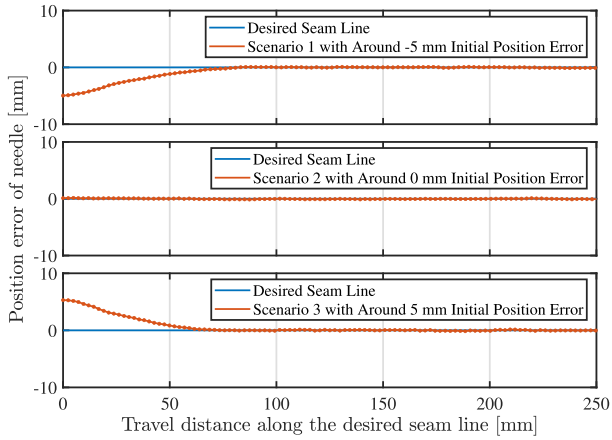

Fig. 7. Seam line trajectories of Sc1–Sc3 with the initial error around −5, 0 and +5 mm and the sewing velocity $\bar{n}_s = 5$ stitches/s.

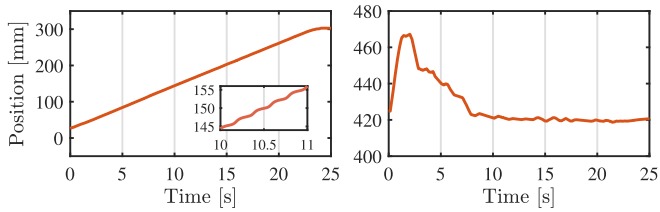

Fig. 8. Observed trajectory of the end-effector of Sc1 in y_w (left) and x_w (right) in the time domain. An enlarged subfigure shows the step-shaped trajectory of the end-effector in y_w.

TABLE II
EXPERIMENTAL CONDITION OF EACH SC

Sc No.	1	2	3	4	5	6	7	8	9
Initial error [mm]	−5	0	+5	−5	−5	−5	−5	0	0
$\bar{n}_s$ [stitches/s]	5	5	5	3	1	5	5	5	1
Seam shape	L	L	L	L	L	L	L	C	C
Control mode	H	H	H	H	H	F	M	H	H

The initial conditions of conducted scenarios (Scs) are presented in Table II. "L" and "C" in seam shape represent linear and curved desired seam lines, respectively. "H," "M," and "F" represent hybrid motion and force control, only motion control and only force control in the sewing direction, respectively. Sc1–Sc3 show the experiments with a linear desired seam line under different initial errors. The comparison of Sc1, Sc4, and Sc5

Fig. 9. Time series images of Sc1 with -5 mm initial needle position error and sewing velocity $\bar{n}_s = 5$ stitches/s.

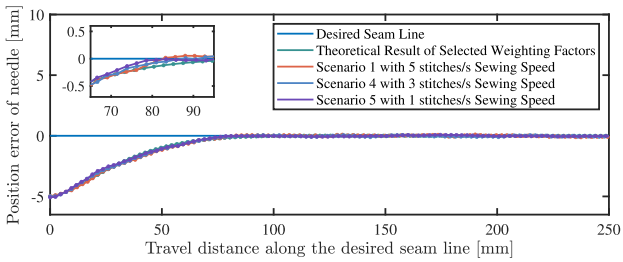

Fig. 10. Trajectories of the theoretical and observed sewn seam lines given the same initial states but different sewing speeds.

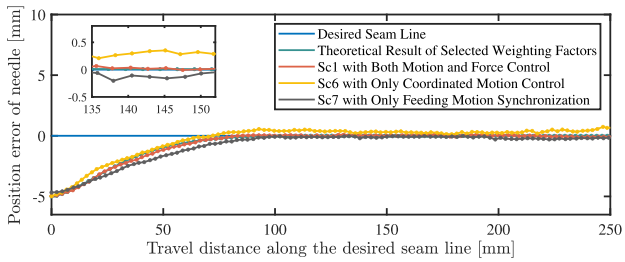

Fig. 11. Trajectories of the theoretical and observed sewn seam lines with different control schemes along the sewing direction.

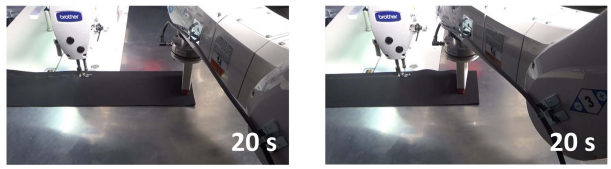

Fig. 12. Sc6 [(a) with only coordinated motion control in y_w] and Sc7 [(b) with only feeding motion synchronization in y_w] with 5 mm initial needle position error and 5 stitches/s sewing speed.

highlights the advantages of time-scaling modeling. Sc1, Sc6, and Sc7 show the necessity of hybrid motion and force control in the sewing direction. Finally, Sc8 and Sc9 are conducted to show the system performance in converging to a curved desired seam line at different $\bar{n}_s$.

At first, to demonstrate the system performance in converging to a linear desired seam line with different initial errors, the scanned photos of Sc1 and seam line trajectories of Sc1–Sc3 are shown in Figs. 6 and 7, respectively. It can be observed that the seam lines are continuous, smooth, and even, without any wrinkles and deformations, and all trajectories converge to the desired seam line without overshoot.

The trajectories of the end-effector in Sc1 in the sewing direction y_w, and the perpendicular sewing direction x_w, are shown in Fig. 8 to demonstrate how the fabric is manipulated. For y_w, the step-shaped trajectory can be observed, with an increase of about 2.4 mm every 0.2 s, which maintains the relative velocity zero between the end-effector and the fabrics. For x_w, two relatively large movements can be observed at the beginning to control the sewn seam line converging to the desired seam line. Subsequently, some adjustments are observed to ensure the convergence.

The time series images of Sc1 are shown in Fig. 9 as an example. It can be observed that, at the beginning of the sewing task, the end-effector manipulates the fabric feed direction, thereby converging the sewing trajectory to the desired seam line. After convergence, the manipulator continues to move forward without any relative movement to the fabric. The fabric remained free of large wrinkles or deformations throughout the process, and the end-effector remained oriented toward the sewing needle point.

To investigate the property of time-scaling modeling, Fig. 10 shows the desired seam line, a theoretical seam line trajectory, and the observed seam line trajectories for Sc1, Sc4, and Sc5. It is shown that all of the seam line trajectories are almost the same with different sewing speeds. This result shows that the proposed time-scaling model-based feedback control in the z_1 domain can be applied to different sewing speeds without changing feedback gain. This property is suitable for industrial applications in the sense that it saves the effort of tuning various control parameters for different sewing tasks.

To show the necessity of the hybrid motion and force control in the sewing direction, Fig. 11 shows the desired seam line, a theoretical seam line trajectory, and the observed seam line trajectories for Sc1, Sc6, and Sc7. Fig. 12 shows two moments of Sc6 and Sc7 during the sewing process. The experimental results show that only the observed seam line trajectory of Sc1 converges to the desired value in almost the same way as the theoretical trajectory. In the case of Sc6, the relative movement between the end-effector and the fabric led to the loss of controllability of the sewing system. In the case of Sc7, large deformations and wrinkles appear between the end-effector and the sewing machine. These results show that coordinated motion control and feeding motion synchronization play important roles in the proposed robotic sewing system to ensure the implementation of time-scaling modeling of the sewing process kinematics and good sewing performance.

To demonstrate the system performance with a curved desired seam line in different sewing speeds, Sc8 and Sc9 are conducted with the scan photo of Sc8 shown in Fig. 6 and both seam line trajectories shown in Fig. 13. The seam line trajectories demonstrate that the proposed robotic sewing system achieves curved seam line sewing with a submillimeter accuracy of less than 0.2 mm deviation from the curved desired seam line. In addition, it can be observed that the seam line trajectory of

TABLE III
SEWING RESULTS IN DIFFERENT SCS

Parameters	Description	Sc1	Sc2	Sc3	Sc4	Sc5	Sc6	Sc7	Sc8	Sc9
μ [mm]	Mean of the stitch size	2.38	2.39	2.37	2.39	2.39	2.27	2.41	2.35	2.37
σ^2 [mm^2]	Variance of the st itch size	0.0024	0.0028	0.0012	0.0019	0.0017	0.0165	0.01867	0.0121	0.0071
$\mathcal{T}_{\text{ave}}$ [N]	Average tension of fabric	1.38	1.35	1.26	1.25	0.58	2.74	0.85	1.33	0.78
$\mathcal{T}_{\text{max}}$ [N]	Maximum tension of fabric	2.96	2.77	2.87	2.48	1.67	5.85	2.88	3.72	2.49

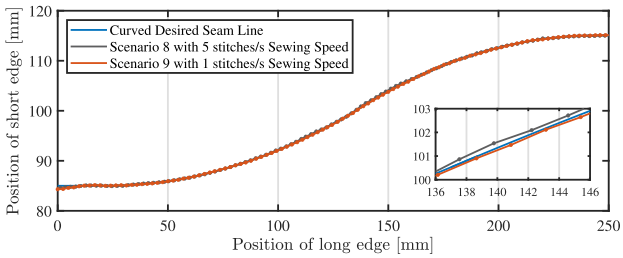

Fig. 13. Seam line trajectories of Sc8 and Sc9 with the sewing velocity $\bar{n}_s = 5$ and $\bar{n}_s = 1$ stitches/s, respectively.

Sc9 with low-speed sewing, $\bar{n}_s = 1$ stitches/s achieved better sewing performance than Sc8 with high-speed sewing, $\bar{n}_s = 5$ stitches/s. The primary reason is that high-speed curved sewing increases the likelihood of inducing slight bending deformations of the fabrics, which consequently affects the estimation of the fabric edge position, thereby impacting the overall sewing accuracy. As a result, it is recommended to reduce the sewing speed to ensure the sewing accuracy and quality of the robotic sewing platform during curved sewing tasks.

Finally, Table III presents the sewing results of stitch size and the observed fabric tension in all Scs. The stitch length is slightly shorter on average than the desired length due to slight puckering of the fabric after sewing. The results demonstrate that the proposed robotic sewing system maintains good sewing performance in Sc1–Sc5. However, without the feeding motion synchronization, Sc6 exhibits the largest $\mathcal{T}_{\text{ave}}$ and $\mathcal{T}_{\text{max}}$. This can be attributed to the largest error in μ observed in Sc6. Furthermore, σ^2 in Sc6 and Sc7 are larger than other linear sewing Scs, resulting in poor sewing performance. Considering Sc8 and Sc9 for curved sewing, low-speed curved sewing shows better performance than high-speed curved sewing in terms of achieving a closer approximation of μ to the desired value and maintaining a smaller σ^2.

VI. CONCLUSION

This article proposed the kinematics modeling of the sewing process as a nonholonomic process. By applying the time-scaling technique, the nonlinear model is precisely linearized in the z_1 domain where z_1 is the distance traveled by the needle along the desired seam line. The efficiency and accuracy of the proposed modeling enable real-time state feedback control of a sewing task. Based on the original industrial sewing machine and inspiration from skilled sewers, the real-time control architecture is proposed, which achieves precise control of the fabric during the sewing task.

Several experiments have been conducted based on the proposed real-time control architecture. The experimental results show high performance of the proposed robotic sewing system with submillimeter accuracy for both linear and curved sewing. Besides, the same sewing results are obtained with different sewing speeds, which shows the application potential of the proposed robotic sewing system for industrial sewing automation in terms of saving the tuning effort of control parameters to obtain precise and robust sewing results in different sewing tasks. In addition, the experimental results show the important role of hybrid motion and force control in the sewing direction. Finally, the impact on sewing speed for curved sewing is discussed.

Future work will focus on the sewing automation of fabrics with complex curved or multiple desired seam lines exhibiting large curvature, which requires more sophisticated task planning and manipulation skills of the robotic sewing platform.

REFERENCES

[1] T. Gries and V. Lutz, "8—application of robotics in garment manufacturing," in *Automation in Garment Manufacturing (The Textile Institute Book)*. Sawston, U.K.: Woodhead Publishing, 2018, pp. 179–197.
[2] P. Taylor and D. Pollet, "Why is automated garment manufacture so difficult ?," in *Proc. IEEE Int. Conf. Adv. Robot.*, 1997, pp. 39–44.
[3] S. Lee et al., "Implementation of an automated manufacturing process for smart clothing: The case study of a smart sports bra," *Processes*, vol. 9, 2021, Art. no. 289.
[4] D. Gershon, "Parallel process decomposition of a dynamic manipulation task: Robotic sewing," *IEEE Trans. Robot. Autom.*, vol. 6, no. 3, pp. 357–367, Jun. 1990.
[5] P. N. Koustoumpardis and N. A. Aspragathos, "Intelligent hierarchical robot control for sewing fabrics," *Robot. Comput. -Integr. Manuf.*, vol. 30, no. 1, pp. 34–46, 2014.
[6] R. C. Winck, S. Dickerson, W. J. Book, and J. D. Huggins, "A novel approach to fabric control for automated sewing," in *Proc. IEEE/ASME Int. Conf. Adv. Intell. Mechatron.*, 2009, pp. 53–58.
[7] J. Schrimpf, M. Bjerkeng, M. Lind, and G. Mathisen, "Model-based feedforward and setpoint generation in a multi-robot sewing cell," in *Proc. IEEE Int. Conf. Robot. Autom.*, 2015, pp. 2027–2033.
[8] J. Schrimpf and L. E. Wetterwald, "Experiments towards automated sewing with a multi-robot system," in *Proc. IEEE Int. Conf. Robot. Autom.*, 2012, pp. 5258–5263.
[9] F. Tokuda, R. Murakami, A. Seino, A. Kobayashi, M. Hayashibe, and K. Kosuge, "A fixture-free 2D sewing system by a dual-arm manipulator and visual feedback control," Nov. 22, 2023, doi: 10.36227/techrxiv.24581706.v1.
[10] H.-T. Lin, "Development of the intelligent pneumatic sewing platform for mask production," *IEEE Access*, vol. 8, pp. 141777–141786, 2020.
[11] S. Ku, H. Choi, H.-Y. Kim, and Y.-L. Park, "Automated sewing system enabled by machine vision for smart garment manufacturing," *IEEE Robot. Autom. Lett.*, vol. 8, no. 9, pp. 5680–5687, Sep. 2023.
[12] N. Kosaka, Y. Chida, M. Tanemura, and K. Yamazaki, "Real-time optimal control of automatic sewing considering fabric geometric shapes," *Mechatronics*, vol. 94, 2023, Art. no. 103005.
[13] T. Shungo and D. Hisashi, "Development of fabric feed mechanism using horizontal articulated dual manipulator for automated sewing," in *Proc. Int. Conf. Autom. Sci. Eng.*, 2021, pp. 1832–1837.
[14] J. Borrás, G. Alenyá, and C. Torras, "A grasping-centered analysis for cloth manipulation," *IEEE Trans. Robot.*, vol. 36, pp. 924–936, Jun. 2020.
[15] M. Sampei and K. Furuta, "On time scaling for nonlinear systems: Application to linearization," *IEEE Trans. Autom. Control*, vol. AC-31, no. 5, pp. 459–462, May 1986.

[16] M. Sampei, "A control strategy for a class of nonholonomic systems—time-state control form and its application," in *Proc. IEEE Conf. Decis. Control*, 1994, pp. 1120–1121.
[17] R. M. Murray, S. S. Sastry, and L. Zexiang, *A Mathematical Introduction to Robotic Manipulation*. Boca Raton, FL, USA: CRC Press, 1994.
[18] K. Kosuge, K. Furuta, and T. Yokoyama, "Virtual internal model following control of robot arms," in *Proc. IEEE Int. Conf. Robot. Autom.*, 1987, pp. 1549–1554.
[19] K. Kosuge, K. Kamei, and T. Nammoto, "Coordinated motion control of dual manipulators for handling a rigid object with non-negligible deformation," in *Proc. IEEE Int. Conf. Robot. Autom.*, 2014, Art. no. 5145.

Kai Tang (Student Member, IEEE) received the B.Sc. degree in process equipment and control engineering from the South China University of Technology, Guangzhou, China, in 2020 and the M.Sc. degree in control system (distinction) from Imperial College London, London, U.K., in 2021. He is currently working toward the Ph.D. degree in control systems with JC STEM Lab of Robotics for Soft Materials, Department of Electrical and Electronic Engineering, The University of Hong Kong, Hong Kong SAR, China.

He is currently with the Centre for Transformative Garment Production, Hong Kong SAR, China. His research include robotics manipulation, control engineering, and learning.

Fuyuki Tokuda (Member, IEEE) received the B.S. degree in engineering from the Nagoya Institute of Technology, Nagoya, Japan, in 2017 and the M.S. and Ph.D. degrees in engineering from Tohoku University, Sendai, Japan, in 2019 and 2022, respectively

From 2022 to 2023, he was a Postdoctoral Fellow with the Centre for Transformative Garment Production, Hong Kong SAR, China. He has been a Research Officer with the Centre for Transformative Garment Production, since 2023, and a Visiting Research Associate with the University of Hong Kong, Hong Kong SAR, China, since 2022. His research interests include robot vision, visual feedback control, robotic assembling, and robotic sewing.

Dr. Tokuda was the recipient of an Outstanding Presentation Award from SICE Tohoku 55th Anniversary Conference in 2020, a research fellowship from the Tohoku University Graduate Program for Integration of Mechanical Systems in 2018, a research fellowship from Japan Society for the Promotion of Science (JSPS) in 2021.

Akira Seino (Member, IEEE) received the B.S. degree in engineering from the Department of the Mechanical System Engineering, Yamagata University, Yamagata, Japan, in 2014 and the M.S. and Ph.D. degrees in engineering from the Department of Bioengineering and Robotics, and the Department of Robotics, Tohoku University, Sendai, Japan, in 2016 and 2019, respectively.

From 2019 to 2021, he was a Project Assistant Professor with the Faculty of Symbiotic Systems Science, Fukushima University, Fukushima, Japan. He was a Research Fellow with Transformative AI & Robotics International Research Center, Tohoku University, Sendai, Japan, in 2019. He is currently a Research Officer with the Centre for Transformative Garment Production, Hong Kong SAR, China, and a Visiting Research Associate with the Department of Electric and Electronics Engineering, The University of Hong Kong, Hong Kong SAR, China. His research interests include mechanical design for robots, robot technology for industrial applications, and control of power-assisted systems.

Dr. Seino is a member of the IEEE Robotics and Automation Society (IEEE RAS).

Akinari Kobayashi (Member, IEEE) received the B.S. and M.S. degrees in engineering and the Ph.D. degree in engineering from Tohoku University, Sendai, Japan, in 2013, 2017, and 2020, respectively.

He has been a Research Officer with the Centre for Transformative Garment Production, Hong Kong SAR, China, since 2021, and a Visiting Research Associate with the University of Hong Kong, Hong Kong SAR, China, since 2022. His research focuses on robot hands, robotic manipulation, and robot sewing.

Dr. Kobayashi is a member of the IEEE Robotics and Automation Society (IEEE RAS).

Norman C. Tien received the B.S. degree in engineering physics from the University of California at Berkeley, Berkeley, CA, USA, in 1981, the M.S. degree in electrical engineering from the University of Illinois, Champaign, IL, USA, in 1984, and the Ph.D. degree in electrical engineering from the University of California at San Diego, La Jolla, CA, USA, in 1993.

He is currently the Taikoo Professor of Engineering and Chair Professor of Microsystems Technology with the University of Hong Kong (HKU), Hong Kong. He is also the Head of Innovation Academy of Faculty of Engineering and the Managing Director of the Centre for Transformative Garment Production. He was the Dean of Engineering from 2012 to 2018, and was the Vice-President and Pro-Vice-Chancellor (Institutional Advancement) from 2019 to 2021 with HKU. Prior to joining HKU, he was the Nord Professor of Engineering with Case Western Reserve University, Cleveland, OH, USA, where he was the Dean of Engineering from 2007 to 2011. He previously held faculty positions with the University of California at Davis, Davis, CA, USA, University of California at Berkeley, Berkeley, CA, USA, and Cornell University, Ithaca, NY, USA. His research interests include micro and nanotechnology, microelectromechanical (MEMS) systems, and robotics.

Kazuhiro Kosuge (Life Fellow, IEEE) received the B.S., M.S., and Ph.D. degrees in control engineering from the Tokyo Institute of Technology, Tokyo, Japan, in 1978, 1980, and 1988, respectively.

He is currently the Chair Professor of Robotic Systems, Department of Electrical and Electronic Engineering, University of Hong Kong, Hong Kong. After having served as an R&D Staff of the Production Engineering Department, Nippon Denso Company, Ltd., Kariya, Japan, a Research Associate with the Tokyo Institute of Technology, and an Associate Professor with Nagoya University, Nagoya, Japan, he joined Tohoku University, Sendai, Japan, as a Professor in 1995 and was a Distinguished Professor from 2018 to 2021. He is currently a Deputy Managing Director of the Centre for Transformative Garment Production, Hong Kong SAR, China, and the Director of the JC STEM Lab of Robotics for Soft Materials, The University of Hong Kong, Hong Kong SAR, China.

Dr. Kosuge was the recipient of the Medal of Honor, Medal with Purple Ribbon, from the Government of Japan in 2018—A national honor in recognition of his prominent contributions to academic and industrial advancements. He was also the recipient of the IEEE RAS George Saridis Leadership Award in Robotics and Automation in 2021 for his exceptional vision of innovative research and outstanding leadership in the robotics and automation community through technical activity management. He is a Japan Society of Mechanical Engineers Fellow, SICE Fellow, Robotic Society of Japan, Society of Automotive Engineers of Japan Fellow, and a member of the Engineering Academy of Japan. He was the President of the IEEE Robotics and Automation Society, from 2010 to 2011, the IEEE Division X Director, from 2015 to 2016, and the IEEE Vice President for Technical Activities for 2020.